Volume 1 | Number 1 | Jan 2013 | Pages 1–100

Dalton Transactions

An international journal of inorganic chemistry
www.rsc.org/dalton

ROYAL SOCIETY OF CHEMISTRY

This is an *Accepted Manuscript*, which has been through the Royal Society of Chemistry peer review process and has been accepted for publication.

Accepted Manuscripts are published online shortly after acceptance, before technical editing, formatting and proof reading. Using this free service, authors can make their results available to the community, in citable form, before we publish the edited article. We will replace this *Accepted Manuscript* with the edited and formatted *Advance Article* as soon as it is available.

You can find more information about *Accepted Manuscripts* in the **Information for Authors**.

Please note that technical editing may introduce minor changes to the text and/or graphics, which may alter content. The journal's standard **Terms & Conditions** and the **Ethical guidelines** still apply. In no event shall the Royal Society of Chemistry be held responsible for any errors or omissions in this *Accepted Manuscript* or any consequences arising from the use of any information it contains.

ROYAL SOCIETY OF CHEMISTRY

www.rsc.org/dalton

Hydration Properties Determining the Reactivity of Nitrite in Aqueous Solution

Saowapak Vchirawongkwin[a], **Chinapong Kritayakornupong**[b], **Anan Tongraar**[c] and **Viwat Vchirawongkwin**[*d]

The knowledge of hydration properties for the nitrite ion is a key to understand its reaction mechanism controlled by the solvent effects. Here, the *ab initio* quantum mechanical charge field molecular dynamics method was performed to acquire the structural and dynamical properties of hydration shell on an aqueous solution of nitrite ion, elucidated by the data analysis with molecular approach and an extended quantitative analysis of all superimposed trajectories with three-dimensional alignment (density map). The pattern of power spectra corresponded with the experimental data, indicating a decency of the Hartree-Fock method coupling with the double-ζ plus polarization and diffuse functions basis sets to study this system. The density maps revealed the structure of hydration shell that there presented a higher density in the $N-O$ bond directions than the vertical axis to the molecular plane, whereas the atomic and molecular radial distribution functions provided the vague information. The number of actual contacts specified 4.6 water molecules interacting with the nitrite ion, and 1.5 extra waters, also located in the molecular hydration shell, forming a H-bonding network with the bulk water. The mean residence times for the water ligands designated the strength of the hydration spheres for the oxygen sites, whilst the results of nitrogen site exhibited an over-counting of waters from other sites and a weak structure. These results evince the influence of water molecules surrounding the nitrite ion, creating an anisotropic hydration shell that it suggests the reactive sites situated above and below its molecular plane via a lower water density.

1 Introduction

All biological processes and most chemical reactions occur in the liquid phase, where the solvent molecules envelop those relevant species. The inevitable effects of solvent contribute in determining the direction, efficiency and rate of a reaction. Numerous biochemical and industrial processes have utilized various anions for, such as, a crystallization and an electron transferring mechanism. One of a common anion is nitrite that it is a reduction product of nitrate ion and employs as a food preservative affecting as an antimicrobial agent[1]. Additionally, the actinide metals, *e.g.* thorium (Th), uranium (U) and neptunium (Np), can form the nitrite complexes, according to the usage of nitric media in the nuclear fuel cycle[2,3]. Although the nitrite ion presents in natural sources having a very small amount, human body can reduce the ingested nitrate to

nitrite in the gastric lumen[4]. It has been reported as a precursor of the carcinogenic N-nitroso compounds causing human cancer[5,6], whilst recent studies on therapeutic usage suggested possible new roles for the nitrite ion in physiology[7,8]. This ion has also found as the intermediary compound in the dissimilatory denitrification by organisms to drive the nitrogen cycle, reducing nitrite ion to nitric oxide via the nitrite reductases (NiRs)[9]. Many recent works studied on the copper-containing NiR (CuNiR), due to variety binding modes between a type 2 copper site and the nitrite ion[10–14]. The crystal structure of CuNiR at 1.4 Å resolution reported the nitrite ion binding to the copper with an almost side-on interaction[10]. The nitro-to-nitrito linkage isomerization occurred in the low-temperature photolysis of the {FeNO}[6] class, indicating diversity interactions between nitrite with iron porphyrins in biological systems[15]. Källrot *et al.* reported the difference in the structure of the catalytic site in the CuNiR determined by the movement of the solvent molecule, revealing a role of solvent effect on this enzyme[11]. From another point of view, we recently reported an anisotropic hydration shell of thiosulfate ion that solvent molecules determines the active site on its terminal sulfur atom[16]. These previous data raise the question of how are solvent molecules determining the involvement of nitrite ion in reactions.

The perception of the structural and dynamical properties

[a] *Department of Pharmaceutical Chemistry, Faculty of Pharmacy, Rangsit University, Patumthani 12000, Thailand.*
[b] *Department of Chemistry, Faculty of Science, King Mongkut's University of Technology Thonburi, Bangkok 10140, Thailand.*
[c] *School of Chemistry, Institute of Science, Suranaree University of Technology and NANOTEC-SUT Center of Excellence on Advanced Functional Nanomaterials, Nakhon Ratchasima 30000, Thailand.*
[d] *Department of Chemistry, Faculty of Science, Chulalongkorn University, Phayathai Road, Patumwan, Bangkok 10330, Thailand. Fax: +66(2)218-7598; Tel: +66(2)218-7633; E-mail: Viwat.V@Chula.ac.th*

Dalton Transactions Accepted Manuscript

for an aqueous nitrite solution can reveal its involvement in chemical and biological reactions. Although the nitrite ion is a common in aqueous solutions, there is only one experiment, in our knowledge, utilizing the time-of-flight neutron diffraction to estimate the hydration number of aqueous sodium nitrite [17]. Recently, Richards *et al.* investigated on the dehydration process for the transport of hydrated nitrite ion through narrow pores by using the molecular dynamics simulation with pair potential function, also predicting an average coordination number with a simple sphere of the hydration shell [18]. Thus, it requires a greater precise method and rigorous data analysis to acquire further feathers in the hydration properties of nitrite ion. An *ab initio* quantum mechanical charge field molecular dynamics (QMCF MD) formalism [19,20], based on a combined quantum mechanics/molecular mechanics (QM/MM) MD approach [21–24], is a promising method to evaluate the properties of aqueous nitrite solution, according to the inclusion of N-body effects describing the interactions between the ion and surrounding water molecules to obtain the hydration structure in the equilibrium state. Moreover, this method has provided successive results when applied on an aqueous solution of numerous anions [16,25–33]. The analysis of vibration spectra can confirm the appropriation of the selected theoretical level in the simulation protocol, by comparing the calculated results with available IR and Raman data. Here, we also extended the analysis techniques to a molecular approach, according to the nitrite ion having geometry causes a complicated hydration structure and two identical oxygen atoms that there are unable to discriminate in an experimental investigation. The quantitative analysis on the superimposed configurations with the three-dimensional alignment can reveal the peculiar characteristics for the hydration structure of nitrite and propose its involvement in a chemical reaction.

2 Methods

We selected the hybrid quantum mechanical and molecular mechanical molecular dynamics (QM/MM MD) simulation to investigate the structural and dynamical properties of nitrite and its hydration shell. However, the conventional QM/MM MD methods include a time-consuming and sometimes hardly manageable task that it is the construction of potential functions between the solute and surrounding water molecules [21–24]. Thus, we applied the *ab initio* quantum mechanical charge field molecular dynamics (QMCF MD) formalism [19,20], by extending the quantum mechanically treated solvent layer beyond the first hydration shell of the solute resulting in negligible non-Coulombic interactions between the solute and bulk water. The details of the QMCF MD framework have been published elsewhere [16,19,20]. A valuable feature of this method is the involvement of the point charges of the atoms in the molecular mechanical (MM) region with their

changing positions in the core Hamiltonian, whilst the dynamically changing charges of QM particles determined by Mulliken population analysis contributed to force on each atom in the MM region as Coulombic forces.

The selection of theoretical level performed the calculations for the QM region is an important task. Here, we emphasize at the single determinant methods, corresponding to a feasible application in the simulation procedure. It is well known that the anion needs diffuse functions to describe the extra electrons within the system, but Howell et al. applied the 6-31G basis set combined with Hartree–Fock (HF) method to the nitrogen and oxygen atoms within the nitrite ion to optimize the geometries of $NO_2^-(H_2O)_n$ $(n = 1 - 3)$ [34]. Banerjee et al. modified the Dunning double-ζ basis set by adding diffuse *s* and *p* functions for nitrogen and a diffuse *p* function for oxygen (modified-DZ) without the polarization, utilized in the Monte Carlo simulation of small hydrate clusters of the nitrite ion [35]. In order to assess a suitable theoretical level, we optimized the free nitrite ion in the gas and the polarizable continuum model (PCM) with various levels by using the Gaussian03 package [36], and reported the structural parameters such as the bond length (d_{N-O}) and bond angle ($\angle ONO$) compared with the experimental data in Table 1. The 6-31G and modified-DZ basis sets combined with the HF method overestimated the bond length comparing with the data of gas phase, but the corresponding PCM results accorded to the value reported from the time-of-flight neutron diffraction on D_2O solutions of 10 mol% $NaNO_2$ [17]. The polarization and diffuse basis sets, namely 6-31+G(d) and DZP+, at the HF level improved the d_{N-O} value close to the gas phase data, comparing with their corresponding simple form. The electron correlation methods, namely the second-order Møller–Plesset (MP2) and the quadratic configuration interaction with single and double excitations (QCISD), again overestimated the bond length in both gas and PCM phases. The structural and dynamical results obtained from previous QMCF MD studies [16,25–33] have indicated the HF method to be a decent compromise between accuracy and affordable computational effort. Moreover, the Dunning double-ζ plus polarization and diffuse functions (DZP+) [38,39] basis sets for nitrogen and oxygen atoms have successfully described the structural and dynamical properties of nitrate ion [32]. Thus, we also utilized the QM calculation at the HF level with the DZP+ basis sets for nitrogen and oxygen atoms of nitrite ion and the Dunning double-ζ plus polarization (DZP) [38,39] basis sets for hydrogen and oxygen atoms of water molecules.

The system consisted of one nitrite ion and 496 water molecules in a cubic box of 24.64 Å with the periodic boundary condition, resulting in a density of 0.997 g cm^{-3} corresponding to the experimental value of pure water at 298 K. The simulation performed in the *NVT* ensemble utilizing a general predictor-corrector algorithm with a time step of 0.2 fs.

Table 1 The bond distances, d_{N-O}, (Å) and bond angle, $\angle ONO$, (deg) within the optimized geometries of NO_2^- ion in gas and PCM phases obtained from various theoretical levels

Theoretical Level	Gas		PCM	
	d_{N-O}	$\angle ONO$	d_{N-O}	$\angle ONO$
HF/6-31G[34]	1.256[34]	117.0[34]	1.254	116.5
MP2/6-31G	1.328	115.4	1.324	115.2
HF/6-31+G(d)	1.225	117.2	1.224	116.8
MP2/6-31+G(d)	1.278	116.0	1.275	115.7
QCISD/6-31+G(d)	1.270	116.3	1.268	115.9
HF/modified-DZ[35]	1.266[35]	117.1[35]	1.263	116.4
MP2/modified-DZ	1.342	115.0	1.336	114.8
HF/DZP+	1.232	116.7	1.231	116.2
MP2/DZP+	1.290	115.0	1.285	114.8
QCISD/DZP+	1.282	115.3	1.278	114.9
G3MP2	1.281	115.4	1.278	115.2
exptl.	1.236[37]	115[37]	1.258 ± 0.006[17]	

The preservation of system temperature at 298.16 K used the Berendsen temperature-scaling algorithm[40] with a relaxation time of 100 fs. Although this temperature-scaling algorithm requires, in principle, a long simulation period to describe the phase space sufficiently, a large number of successful publications of QMCF MD simulations[16,25–33] indicate that the simulation period of 10 ps is adequate to reproduce the properties of hydrated ions well. The QM subregions, namely the core and layer zones, extended to 3.2 and 6.8 Å, respectively, corresponding to the nitrate system[32]. This size of QM region contained 37.4 water molecules as the average value during the simulation period. The thickness of the smoothing region was 0.2 Å inside from the QM radius with the values of r_{on} and r_{off} as 6.6 and 6.8 Å, respectively, according to the radial distribution function (RDF) obtained from the equilibrated simulation. The selected water model including an intramolecular potential to calculate the interactions between pairs of water in the MM region was the flexible BJH–CF2 model[41,42], with the cutoff distances of 3.0 and 5.0 Å for non-Coulombic interactions between H atoms and between O and H atoms, respectively. This water model assigns the partial charges for oxygen and hydrogen atoms to be -0.65966 and $+0.32983$, respectively, for the water molecule within the MM region and supports the fully flexible molecular geometries of water molecules transiting between the QM and MM region. The Coulombic interactions between the Mulliken charges on the atoms within the QM region and the point charges of water molecules according to the BJH–CF2 model provide an electrostatic description for a dynamically charging field of point charges, according to the movements of atoms inside the QM region and water molecules within the MM region during the simulation. This ensures the continuous adaptation of the Coulombic interactions to all polarization and charge-transfer

effects within solute and surrounding solvent layers.[19,20] In addition, the reaction field method combined with the shifted-force potential technique accounted for the long-range electrostatic potentials and forces, with a spherical cutoff limit of 12.350 Å. We equilibrated the system with the QMCF MD method for 50,000 steps (10 ps), and further collected 50,000 steps (10 ps) as data sampling for analyzing the structural and dynamical properties.

In this work, we evaluated the structural and dynamical properties for the hydration shell of nitrite ion in both atomic and molecular approaches such as the molecular RDFs, molecular coordination number distribution (CND), and molecular ligand mean residence time (MRT). The definition of the molecular hydration shell is the combination of all atomic hydration spheres for the coordinating sites of nitrite ion, producing the molecular domain[43]. The coordinating site for each water molecule to the nitrite is the shortest distance between the oxygen atom of a water molecule and each atom within the ion[29,31]. We calculated all MRT values based on the direct method[44], counting the water exchange processes between hydration shell and bulk. The most appropriate time span to record a water displacement from its original coordination sphere as an exchange process is 0.5 ps[44,45], which corresponds to the average lifetime of a hydrogen bond in the solvent[46].

The velocity autocorrelation function (VACF) is one method to evaluate the dynamical properties of a fluid system related to macroscopic transport coefficients, and the association with normal-coordinate analysis and Fourier transformation yielding the vibrational spectrum[47]. The definition

of normalized VACF, $C(t)$, is

$$C(t) = \frac{\sum_i^{N_t} \sum_j^N v_j(t_i) v_j(t_i+t)}{N_t N \sum_i^{N_t} \sum_j^N v_j(t_i) v_j(t_i)}, \qquad (1)$$

where N is the number of particles, N_t is the number of time origins t_i, and v_j denotes a certain velocity component of the particle j. A correlation length of 2.0 ps was used to obtain the power spectra with 4000 averaged time origins.

3 Results and Discussion

3.1 Structural and Dynamical Properties of NO_2^- Ion

The dynamic movement of all atoms within the nitrite ion throughout the simulation period resulted in the variations of $N-O$ bond distances and $\angle ONO$ angle, shown in Figure 1. The $N-O$ bonds stretch in the range of 1.160 to 1.320 Å with the average values of 1.230 ± 0.023 and 1.232 ± 0.021 Å for each bond. The average $\angle ONO$ angle is $116° \pm 2°$, locating in the range of $109°$ to $123°$. These structure parameters utilized to construct the average geometry of the ion and its geometry shown in Figure 2. The average $N-O$ distances obtained from the QMCF MD are shorter by *ca.* 0.03 Å than the value reported from the time-of-flight neutron diffraction $(1.258 \pm 0.006$ Å$)$ [17]; however, the variation of bond distances in Figure 1a spreads over that experimental value. This confirms the adequacy of selected theoretical level to acquire the structural properties of hydrated nitrite ion.

The symmetry of nitrite ion is the C_{2v} consisting of three vibration modes, spanning into two types of symmetry species as the following representation:

$$\Gamma(C_{2v}) = 2a_1(R, IR) + b_2(R, IR). \qquad (2)$$

The free nitrite ion in 5.8 M aqueous $NaNO_2$ solutions generates three coincident infrared and Raman spectra at 1331, 817 and 1242 cm^{-1} corresponding to symmetric stretch, $v_s(a_1)$, deformation, $\delta(a_1)$, and antisymmetric stretch, $v_{as}(b_2)$, respectively [48]. The calculated spectra from the QMCF MD results shows in a form of broad band, reflecting the dynamic movements of molecular geometry during the simulation period. The width of spectra band is 300 cm^{-1} (1,400 to 1,700 cm^{-1}), 140 cm^{-1} (830 to 970 cm^{-1}) and 390 cm^{-1} (1,370 to 1,780 cm^{-1}) for v_s, δ and v_{as} modes, respectively. Figure 3 displayed all power spectra of the ion, and the assigned frequencies by the highest peak for each mode listed in Table 2 also presenting the scaled values in parentheses by the factor of 0.902 obtained from the correction with the coupled-cluster singles and doubles (CCSD) level [26]. A higher frequency of v_s than the v_{as} mode agrees with the peak assignments in the experiments [48–50]. Table 2 also reported the frequencies, calculated from the optimized geometry of free nitrite ion the
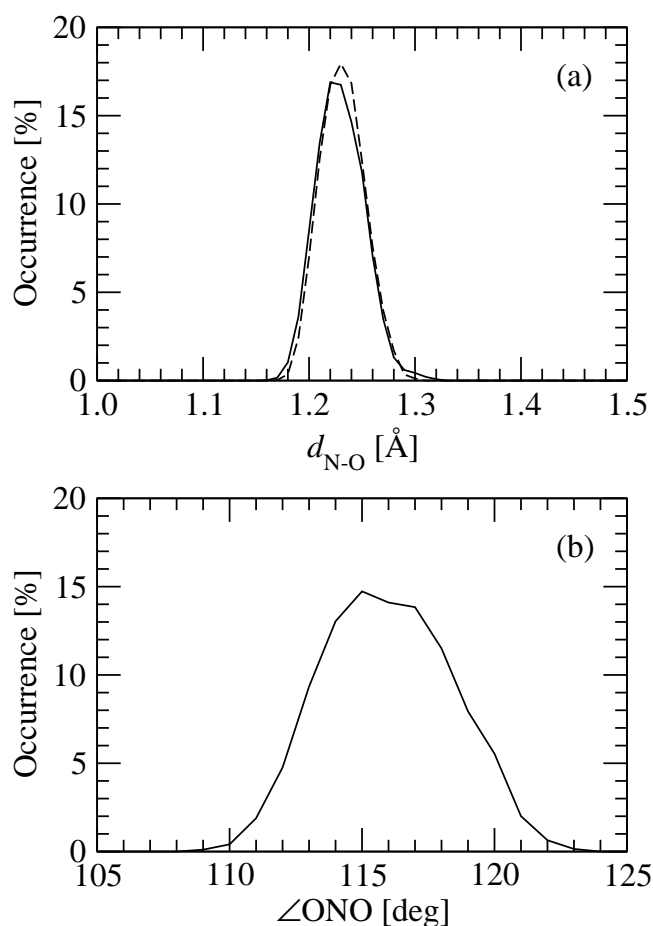
Fig. 1 Distribution of (a) $N-O$ bond lengths (d_{N-O}): the solid- and dashed-line refer to the $N-O(1)$ and $N-O(2)$ bond, respectively, and (b) $O-N-O$ angle ($\angle ONO$) of an aqueous NO_2^- ion obtained from the QMCF MD simulation.

specific theoretical levels in the gas and PCM phases. Interestingly, the MP2 method predicted the reverse order providing a higher frequency of v_{as} than the v_s in the gas phase and also in the PCM phase for 6-31G, 6-31+G(d) and modified-DZ basis sets. The frequency assignments of QMCF MD result agreed with the values calculated by G3MP2 in the PCM phase; however, these values are higher than the experimental data. The G3MP2 overestimated the bond length shown in Table 1 according to that geometry obtained from the MP2(full)/6-31G(d) level [51], but it calculated the vibration frequencies from the optimized geometry by the HF with the basis set within the G3 theory [51] that it underestimated the bond length to be 1.227 Å. Although the G3MP2 level gave the significant higher frequencies than the experimental data, the different frequency between the v_s and v_{as} modes ($v_s - v_{as}$) in the PCM phase agrees with Raman results representing the similar pattern, whilst other theoretical methods predicted the uncor-

Table 2 Vibration frequencies (cm^{-1}) of the highest peak for each normal mode of NO_2^- ion evaluated by the VACFs of QMCF MD simulation, comparing with the experimental data and calculated results at various theoretical levels.

	vibration mode of NO_2^- ion[a]			$\nu_s - \nu_{as}$
	ν_s	δ	ν_{as}	
	Experimental data			
solid $NaNO_2$[b]	1329	829	1232	97
solid KNO_2[b]	1322	806	1240	82
solid $CsNO_2$[b]	1317	803	1230	87
$Ba(NO_2)_2 \cdot H_2O$[c]	1328	820	1240	88
aqueous $NaNO_2$[d]	1331	817	1242	89
	Theoretical results[e]			
HF/6-31G	1449 [1446]	836 [833]	1354 [1400]	95 [46]
MP2/6-31G	1212 [1202]	733 [729]	1340 [1370]	−128 [−168]
HF/6-31+G(d)	1581 [1577]	893 [889]	1457 [1535]	124 [42]
MP2/6-31+G(d)	1329 [1312]	789 [782]	1352 [1395]	−23 [−83]
QCISD/6-31+G(d)	1344 [1333]	791 [782]	1235 [1288]	109 [45]
HF/modified-DZ	1458 [1418]	820 [812]	1262 [1356]	196 [62]
MP2/modified-DZ	1201 [1185]	720 [712]	1274 [1335]	−73 [−150]
HF/DZP+	1635 [1584]	908 [879]	1427 [1521]	208 [63]
MP2/DZP+	1356 [1315]	823 [772]	1310 [1363]	46 [−48]
QCISD/DZP+	1346 [1334]	780 [771]	1190 [1241]	156 [93]
G3MP2	1610 [1608]	896 [893]	1527 [1579]	83 [29]
	QMCF MD results[f]			
NO_2^- $(H_2O)_{496}$	1612 (1454)	896 (808)	1531 (1381)	81 (73)

[a] Notation of vibration modes: stretching (ν); bending (δ); symmetric (subscript s); asymmetric (subscript as).
[b] Raman data of solid [49].
[c] Raman data of polycrystalline $Ba(NO_2)_2 \cdot H_2O$ [50].
[d] Raman data of 5.8 mol·dm^{-3} aqueous $NaNO_2$ solution [48].
[e] The values obtained from the optimized geometry with the specified method in the PCM and the corresponding values for the gas phase presented in the square bracket.
[f] The values in parentheses were scaled by the factor 0.902 [26].
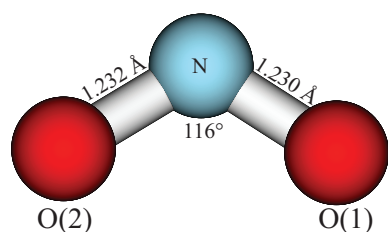
Fig. 2 The averaged geometry of NO_2^- ion constructed from the structural parameters of QMCF MD simulation.

related values. The assigned frequencies in the QMCF MD simulation differed from the result calculated at the HF/DZP+ level, indicating the effect of water molecules within the vicinity of nitrite ion on its internal interactions. The $\nu_s - \nu_{as}$ value of QMCF MD simulation resembled the G3MP2 result and agreed with those from the experimental data. This again con-

firms that the selected theoretical level suited the quantum calculations in QMCF MD simulation for the aqueous nitrite system, and provided relative reliability via the comparable pattern of vibrational spectra with the experimental data.

3.2 Structural and Dynamical Properties of the Hydration Shell

The boundary of atomic hydration spheres is the fundamental information, classifying the water molecules within the hydration shell from the bulk for further analysis similar to other polyatomic solutes [16,29,31–33]. The atomic RDF gives the hydrating structure around each atom within the solute, scanning a number of water molecules based on a simple sphere model. Figure 4 presented atomic RDFs for each site of nitrite ion with oxygen and hydrogen atoms of water via the dashed lines. Interestingly, the atomic $N \cdots O_{water}$ RDF has two peaks located at 3.56 Å and 3.80 Å with the first mini-
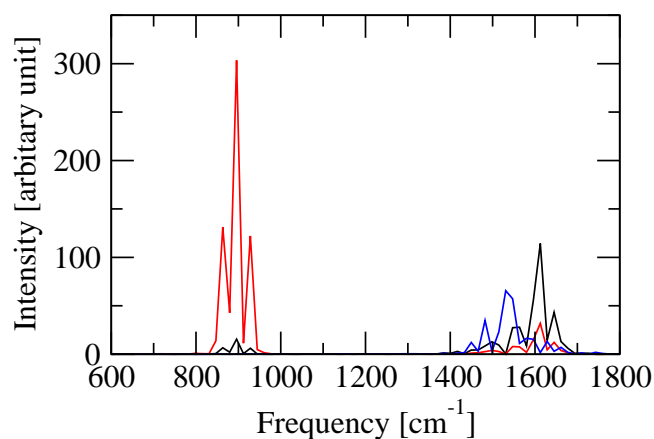
Fig. 3 Power spectra of symmetric N – O stretching (ν_s), ∠ONO bending (δ) and asymmetric N – O stretching (ν_{as}) modes represented with solid black, red and blue lines, respectively.

Fig. 4 The atomic and isolated RDFs plots of (a) N, (b) O(1) and (c) O(2) sites. The black and red lines refer to the RDFs for the O and H atoms of water while the dashed and solid lines present the atomic and isolated RDFs, respectively.

mum situated at 4.48 Å, whilst other atomic O···O_{water} RDFs show a dominant peak with a more contracted hydration by a shorter radius of hydration spheres at the first minimum of 3.58 Å and 3.46 Å for O(1) and O(2) site, respectively. This situation implies a stronger interaction of N site with hydration shell than other two O sites, but it is a contradiction with the O favors in the NO_2^- : H_2O potential energy surface reported by Banerjee et al.[35] We further analyzed the isolated hydration shells via specifying the water molecules of which atom in the solute is the coordinating site, calculating the distances between the oxygen of water and each atom within the nitrite ion and searching the shortest value to define the location. According to all atoms in the simulation box move along the gradient of forces during the simulation period, thus the isolated hydration shells displayed in Figure 5 established by the superimposed configurations with the three-dimensional (3D) alignment by using the contravariant transformation to rotate the inner molecular reference frame of the nitrite ion in each configuration to the Cartesian reference frame[16,33]. Figure 5 represents the qualitative point of view that the O sites allocate larger hydration region than the N site, indicating a stronger interactions with water molecules of former sites than latter site. From a quantitative point of view, we evaluated the RDFs from these isolated hydration shells, called the isolated RDFs, and also displayed in Figure 4 via the solid lines. The isolated RDFs of N atom established a significant difference pattern from its atomic RDFs found the first minimum at 3.68 Å, whilst the first peaks for each isolated RDFs of O sites are similar to the corresponding atomic RDFs. The coincidence of both atomic and isolated RDFs in the short radius of hydration sphere shows that the water molecules in these regions specify coordination to the site, but the separated regions elucidate the collection of water molecules of other sites in the
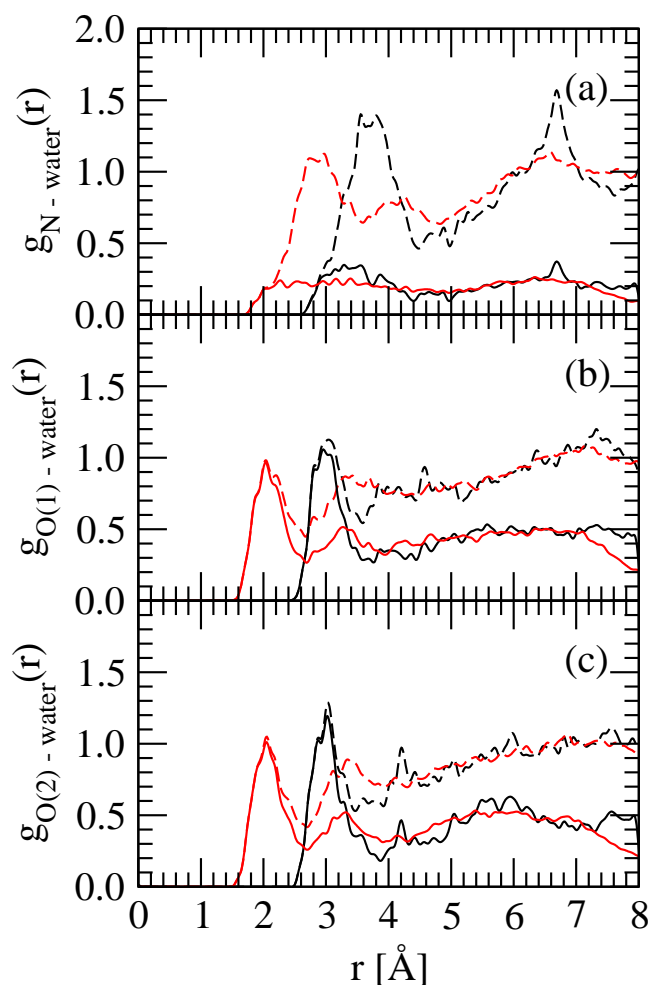
calculated procedure of atomic RDF. It indicates sophistication of hydration shell for the N site with a contribution of water molecules from other coordinating sites in its atomic RDFs. We clarified this complexity via calculating the average density of oxygen and hydrogen around the nitrite ion for each grid in the spherical polar coordinate, constructed by a dividing volume via scanning an increment of r, θ and ϕ to be 0.05 Å, 1° and 1°, respectively. The projection of density onto the (r, θ) and (r, ϕ) planes produces the density maps, illustrating in Figure 6 that it classified the explicit densities of oxygen and hydrogen around the nitrite ion. The density maps show geometry of molecular hydration shell, corresponding to the previous proposal based on the union of spheres[43]. The density maps suggest a more orderly hydration structure of O sites than the N site, according to a higher density around

(a)

(b)

(c)

(d)
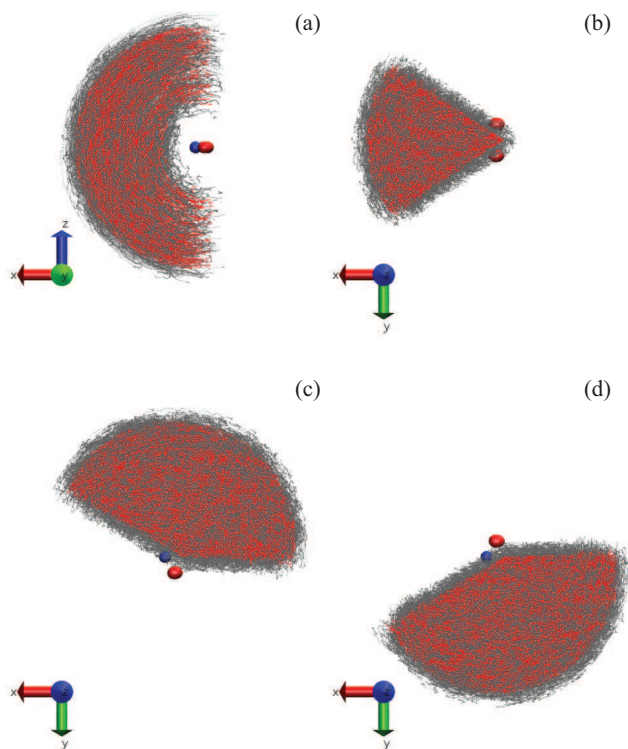
Fig. 5 Spherical sections of hydration shells with the radius of 8 Å from each coordinating site presented via 3D alignment for (a) side-view of N, (b) top-view of N, (c) top-view of O(1), and (d) top-view of O(2). The blue and red spheres are nitrogen and oxygen atoms of NO_2^- ion, respectively, red and gray dots are oxygen and hydrogens of waters.

Table 3 Characteristic values of the radial distribution function $g_{\alpha\beta}(r)$ for each site of NO_2^- ion in the hydration shell determined by the QMCF MD simulation

coordinating site	$r_{max}(O_w)^a$	$r_{min}(O_w)^a$	$r_{max}(H_w)^a$	$r_{min}(H_w)^a$	n^a
N	3.28	3.68	2.26	2.40	3.2
O(1)	2.96	3.44	2.04	2.68	2.7
O(2)	3.00	3.48	2.04	2.70	2.8
Surface	3.02	3.76	2.04	2.70	6.1

a r_{max} and r_{min} are the distances of the maximum and minimum of $g_{\alpha\beta}(r)$ for the hydration shell in Å, and n is the averaged coordination numbers of the shell, respectively.

the former than the latter. This indicates a deficiency in the solitary usage of atomic RDFs to interpret the boundary of the hydration shells. The density maps in the (r, θ) plane, shown in Figure 6a and Figure 6c, distinguish the densities between parallel and perpendicular to the molecular plane of nitrite ion, displaying lower densities in the vertical axis than the atomic directions. This infers the weak interactions of water molecules locating above and below the molecular plane of nitrite ion, but the ion establishes in-plane stronger interactions with water molecules. The density map of oxygen on the (r, ϕ) plane, shown in Figure 6b, clarify the occurrence of double peaks in the atomic RDF of N site, according to the distances of high densities for an encounter of water molecules coordinating with the O sites especially around 90°, 180° and 270° to be close to those in the N site (around 0°).

According to an aforementioned discussion with the precise analysis of hydration shell, we summarized the position of the first peak and its boundary for $(site) \cdots O_{water}$ and $(site) \cdots H_{water}$ RDFs for the nitrite ion in Table 3. The evaluation of the atomic coordination numbers (CNs) utilized the

position of the atomic hydration boundary obtained from its $(site) \cdots O_{water}$ RDF, also listed in Table 3. However, the direct sum of CNs deceives the interpretation of the CN of solute via the over-counting of water molecules within the intersection of atomic hydration spheres[29]. We applied the molecular approach to evaluate the RDFs and CN for the nitrite ion, presented in Figure 7. The molecular RDFs provide the possibility to find water molecules within the isotropic molecular domain constructed from the union of spheres having identical radii[43], by assigning the coordinating site with the shortest distance among the values obtained from the oxygen of water and each site within the nitrite ion. The molecular RDFs of nitrite ion in Figure 7a display a well-defined hydration structure. The difference between the first peak of $(molecular) \cdots O_{water}$ and $(molecular) \cdots H_{water}$ RDFs (0.98 Å) corresponds to the average length of $O-H$ bonds (0.96 ± 0.03 Å) within water molecules located in the molecular hydration shell, indicating the orientation of water molecules utilizing one hydrogen atom to coordinate with the ion. Figure 7b exhibited the molecular CND evaluated by the molecular domain, constructed by applying the boundary obtained form the atomic RDFs for each site of the nitrite ion[43]. The possible CNs of nitrite are in a range of 3 to 10 with a dominant value of 6. We also reported the characteristic values of molecular hydration shell and its average CN from the molecular RDFs and CND in Table 3. The lesser value of molecular CN than the direct sum of all atomic CNs (8.7) is 2.6 molecules, indicating the location of some water molecules in the intersection of the atomic hydration spheres. This molecular CN is twofold lower than the value obtained from the classical MD (12.7)[18], due to a different approach to calculate the values. We got the average value of 11.0 when applied the identical criterion with Richards et al. defining the molecular hydration shell as the radius of 5.0 Å from the N atom[18] to evaluate the CN, suggesting the contribution of high-order repulsive terms in the QM calculations of solute-solvent interactions. The lower molecular CN of nitrite than the nitrate ion (7.9)[32] agrees with the result obtained from the classical MD simulations[18]. The difference of their molecular CN suggests that the nitrite re-
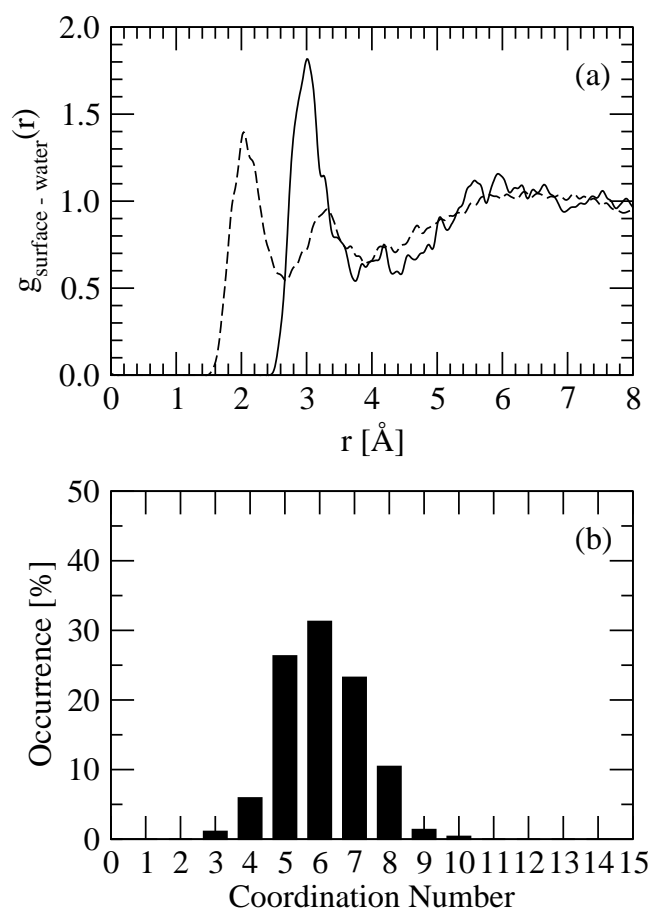
Fig. 7 (a) Molecular RDF plots of NO_2^- ion obtained from the QMCF MD simulation evaluated by the molecular domain; solid and dashed lines refer to the RDF for the O and H atoms of water, respectively. (b) The molecular hydration shell coordination number distribution of the ion.

veals a weaker hydration structure than the nitrate ion, but this is contradiction with the data of hydration free energies reporting the values of -330 and -300 kJ mol^{-1} for the nitrite and nitrate ion[52], respectively. The positions of peaks and hydration boundaries for the atomic RDFs clarify that the water molecules exhibit a more contracted hydration spheres around the nitrite than the nitrate ion[32], supporting a higher thermodynamic stability of hydration shell of the former than the latter ion[52].

A further feature of structural properties is an actual CN, being the number of H-bonds forming between the solute and water molecules via a geometric criterion. The number of actual contacts distinguishes some extra waters from the calculated value obtained by the molecular CND, forming the H-bonding network between the molecular hydration shell and bulk. We defined the actual contact as a suitable orientation of

a water molecule to form the H-bond, depending on the cutoff parameters in analogy to water–dimethyl sulfoxide[53] and our previous studies[31–33]. The cutoff distances $R_{OO}^{(c)}$ and $R_{OH}^{(c)}$ for each oxygen site correspond to the boundary of atomic hydration spheres obtained from (site)$\cdots O_{water}$ and (site)$\cdots H_{water}$ RDFs, respectively. We also defined the cutoff distances of N site, namely the $R_{NO}^{(c)}$ and $R_{NH}^{(c)}$, with the boundary of hydration sphere from its isolated RDFs at 3.68 and 2.40 Å, respectively. The angle $\varphi^{(c)}$ was set to $30°$[53]. Table 4 listed the average number of H-bonds for each site and the molecular hydration (surface) of the nitrite ion. The H-bonds of the surface is the average value of the summation of all H-bonds in each time step over the simulation period. The equality between the di-

Table 4 Average number of hydrogen bonds for each coordinating site and molecular hydration of NO_2^- ion in the simulation period.

coordinating site	H-bonds
N	0.5 ± 0.6
O(1)	2.0 ± 0.8
O(2)	2.1 ± 0.9
surface	4.6 ± 1.3

rect sum of each site and the surface values signifies the ratio 1:1 for the formation of a H-bond between the water molecule and the coordinating site, resulting in the actual contacts of 4.6 and 1.5 extra water molecules located in the molecular hydration without forming the direct interaction to the ion. This actual CN agrees with the value (3.7 ± 0.5) reported from the time-of-flight neutron diffraction[17]. For N site, a large difference between the atomic CN (3.2) and the H-bonds indicates substantial interactions from other sites, attracting some water molecules to allocate a position within the vicinity of this site. This confirms a dominant role of oxygen atoms within an oxoanion to establish the coordination with water molecules in an aqueous solution, evincing a larger number of molecular CN of nitrate (7.9)[32] than the nitrite ion (6.1). The nitrite ion also exhibits a stronger interactions between O sites than those within the nitrate ion via a larger average number of H-bonds for each O site than the nitrate (1.8)[32], supported by the data of hydration free energies[52] and the fact that the former ion is a stronger base than the latter ion.

The investigation of dynamical property for water molecules within the hydration shell employs the ligand MRT calculated by the direct method[44], dividing the average number of water molecules within the hydration shell throughout the simulation period by the number of exchange events with two time parameters ($t^* = 0.0$ and 0.5 ps) corresponding to all displacements and to sustainable exchange events[46]. Table 5 listed MRT values for all coordinating sites and molecular hy-

Table 5 Mean ligand residence time τ (ps), number of accounted ligand exchange events N and total number of processes needed for one successful water exchange R_{ex} obtained from the QMCF MD simulation

	$t^* = 0.0$ ps			$t^* = 0.5$ ps			$R_{\text{ex}}{}^d$
	$N_{\text{inv}}{}^a$	$N_{\text{ex}}^{0.0}/10\text{ ps}^b$	$\tau_{\text{D}}^{0.0c}$	$N_{\text{inv}}{}^a$	$N_{\text{ex}}^{0.5}/10\text{ ps}^b$	$\tau_{\text{D}}^{0.5c}$	
			NO_2^-				
N	29	438	0.08	8	17	2.02	25.8
O(1)	25	155	0.21	13	25	1.30	6.2
O(2)	25	153	0.19	10	20	1.44	7.6
Surface	32	263	0.24	20	34	1.86	7.7
			Pure water				
H_2O^e		269[44]	0.2[44], 0.33[45]		24[44]	1.7[44], 1.51[45]	11.2[44]
H_2O		131[f]	0.2[f], 0.55[46]		20[f]	1.3[f]	6.5[f]

[a] Number of ligand involved in the MRT evaluation according to the value of t^*.
[b] Number of accounted exchange events per 10 ps lasting at least 0.0 and 0.5 ps, respectively.
[c] Mean residence time determined by the direct method [44] in picoseconds.
[d] Average number of processes needed for one successful ligand exchange.
[e] Values obtained from a QM/MM-MD simulation of pure water [44,45] in picoseconds.
[f] Unpublished results: values obtained from a QMCF MD simulation of pure water in picoseconds.

dration shell (surface) for the nitrite ion, compared with the data of pure water simulations [44,45]. The number of involved ligands (N_{inv}) represents the coordination of water molecules with the evaluated site in the criterion of t^*, whilst the number of accounted exchange events (N_{ex}) accumulates the exchange process of N_{inv} throughout the simulation period. The hydrogen bond lifetimes can be estimated with $t^* = 0.0$ ps [29,44], and the standard relaxation time utilized in the direct method with $t^* = 0.5$ ps leads to the MRT of water ligands at the coordinating sites. The $\tau_{\text{D}}^{0.0}$ of N site revealed a remarkably short lifetimes for the formation of H-bonds with water molecules, but it had the longest atomic MRT value. This peculiar property referred to the confined water molecules within the intersection volumes of atomic hydration spheres around the N site, illustrated in Figure 8 as both the superimposed trajectories with 3D alignment based on the contravariant transformation [33] and distances plot for the selected water molecule from each coordinating site. The water rapidly changed the coordinating sites between O(1) (red solid line) and O(2) (blue solid line) during 2.8 to 7.4 ps through the intermediate distances placed within the hydration sphere of N site, presenting the location of this water within the intersection volume of the atomic hydration spheres. This clarifies an overestimation of atomic MRT for the N site and presents the migration of a water molecule within the molecular hydration shell among coordinating sites. The direct sum of atomic $N_{\text{ex}}^{0.5}$ is 56 processes suggesting the migration of water molecules among the coordinating sites to be 22 processes, referring to the confined waters within the molecular hydration shell and reflecting a longer MRT of the molecular hydration than each oxygen site. The atomic MRTs

of O sites for the nitrite ion reveal a stronger H-bonds with surrounding water molecules than the nitrate ion. Moreover, a lower molecular N_{ex} of nitrite also indicates a stronger hydration shell than that of nitrate ion (molecular $N_{\text{ex}} = 44$) [32], supported by a contracted hydration shell from the RDFs and thermodynamics data [52]. Thus, we classify the nitrite ion as a structure-maker, exhibiting a slightly stronger characteristic than the nitrate ion. The number of processes needed for one successful water exchange, R_{ex}, being the ratio of $N_{\text{ex}}^{0.0}$ to $N_{\text{ex}}^{0.5}$, also presents a complexity of the exchange process, according to the significant difference between the atomic and molecular R_{ex} especially for the N site. The R_{ex} for the interchanging of coordinating site within the molecular hydration shell was 21.7, suggesting a localization of water molecules around the coordinating site and most of the exchange processes occurring between the molecular hydration shell and the bulk.

4 Conclusion

In summary, we performed the QMCF MD simulation on the aqueous solution of the nitrite ion to investigate the influence of explicit waters on the structural and dynamical properties of the ion and its hydration shells. A comparable pattern of calculated spectra with the experimental data indicated propriety of the selected theoretical level utilized in the quantum calculations. An extended method in a quantitative view of the superimposed configurations with the three-dimensional alignment or the density map clarified the vague information, obtained from the atomic and also molecular approaches in

Dalton Transactions Accepted Manuscript

the RDF analysis. Moreover, it exposed an anisotropic structure of molecular hydration shell between parallel and perpendicular to the molecular plane of nitrite ion. The agreement of H-bonds result with the thermodynamics data indicated a stronger interactions of oxygens within the nitrite with surrounding waters than those of the nitrate ion[32]. These results signify the role of waters shielding their coordinating site in the $N-O$ bond directions of nitrite ion, whilst the hydration shell determines the reactive sites located above and below the vicinity of its molecular plane. This provided a new insight of the solvent effects to achieve the involvement of this ion in a chemical reaction and various coordination complexes, *e.g.*, nitro- and nitrito-complex.

Acknowledgments

References

1 N. Benjamin, *Ann. Zootech.*, 2000, **49**, 207–216.

2 G. B. Andreev, N. A. Budantseva, I. G. Tananaev and B. F. Myasoedov, *Inorg. Chem.*, 2008, **47**, 2943–2945.

3 F. Dulong, J. Pouessel, P. Thuéry, J.-C. Berthet, M. Ephritikhine and T. Cantat, *Chem. Commun.*, 2013, **49**, 2412–2414.

4 C. Mackerness and C. W. Keevil, in *Origin and significance of nitrite in water*, ed. M. J. Hill, Woodhead Publishing, Cambridge England, 1996, ch. 4, pp. 77–92.

5 N. S. Bryan, D. D. Alexander, J. R. Coughlin, A. L. Milkowski and P. Boffetta, *Food Chem. Toxicol.*, 2012, **50**, 3646–3665.

6 A. Cockburn, G. Brambilla, M.-L. Fernndez, D. Arcella, L. R. Bordajandi, B. Cottrill, C. van Peteghem and J.-L. Dorne, *Toxicol. Appl. Pharmacol.*, 2013, **270**, 209–217.

7 J. O. Lundberg, E. Weitzberg and M. T. Gladwin, *Nat. Rev. Drug. Discov.*, 2008, **7**, 156–167.

8 A. R. Butler and M. Feelisch, *Circulation*, 2008, **117**, 2151–2159.

9 A. C. Merkle and N. Lehnert, *Dalton Trans.*, 2012, **41**, 3355–3368.

10 E. I. Tocheva, F. I. Rosell, A. G. Mauk and M. E. P. Murphy, *Science*, 2004, **304**, 867–870.

11 N. Källrot, K. Nilsson, T. Rasmussen and U. Ryde, *Int. J. Quantum Chem.*, 2005, **102**, 520–541.

12 H. Yokoyama, K. Yamaguchi, M. Sugimoto and S. Suzuki, *Eur. J. Inorg. Chem.*, 2005, **2005**, 1435–1441.

13 R. Silaghi-Dumitrescu, *J. Inorg. Biochem.*, 2006, **100**, 396–402.

14 S. Ghosh, A. Dey, Y. Sun, C. P. Scholes and E. I. Solomon, *J. Am. Chem. Soc.*, 2009, **131**, 277–288.

15 I. V. Novozhilova, P. Coppens, J. Lee, G. B. Richter-Addo and K. A. Bagley, *J. Am. Chem. Soc.*, 2006, **128**, 2093–2104.

16 M. Trinapakul, C. Kritayakornpong, A. Tongraar and V. Vchirawongkwin, *Dalton Trans.*, 2013, **42**, 10807–10817.

17 Y. Kameda, H. Arakawa, K. Hangai and O. Uemura, *Bull. Chem. Soc. Jpn.*, 1992, **65**, 2154–2156.

18 L. A. Richards, A. I. Schfer, B. S. Richards and B. Corry, *Small*, 2012, **8**, 1701–1709.

19 B. M. Rode, T. S. Hofer, B. R. Randolf, C. F. Schwenk, D. Xenides and V. Vchirawongkwin, *Theor. Chem. Acc.*, 2006, **115**, 77–85.

20 T. S. Hofer, A. B. Pribil, B. R. Randolf and B. M. Rode, *Combining Quantum Mechanics and Molecular Mechanics. Some Recent Progresses in QM/MM Methods*, Academic Press, 2010, vol. 59, pp. 213–246.

21 A. Warshel and M. Levitt, *J. Mol. Bio.*, 1976, **103**, 227–249.

22 M. J. Field, P. A. Bash and M. Karplus, *J. Comput. Chem.*, 1990, **11**, 700–733.

23 J. Gao, *J. Am. Chem. Soc.*, 1993, **115**, 2930–2935.

24 D. Bakowise and W. Thiel, *J. Phys. Chem.*, 1996, **100**, 10580–10594.

25 V. Vchirawongkwin, B. M. Rode and I. Persson, *J. Phys. Chem. B*, 2007, **111**, 4150–4155.

26 V. Vchirawongkwin and B. M. Rode, *Chem. Phys. Lett.*, 2007, **443**, 152–157.

27 A. B. Pribil, T. S. Hofer, B. R. Randolf and B. M. Rode, *J. Comput. Chem.*, 2008, **29**, 2330–2334.

28 A. B. Pribil, T. S. Hofer, V. Vchirawongkwin, B. R. Randolf and B. M. Rode, *Chem. Phys.*, 2008, **346**, 182–185.

29 V. Vchirawongkwin, A. B. Pribil and B. M. Rode, *J. Comput. Chem.*, 2010, **31**, 249–257.

30 V. Vchirawongkwin, C. Kritayakornupong, V. Ruangpornvisuti and B. M. Rode, *J. Mol. Struct. (Theochem)*, 2009, **913**, 236–239.

31 V. Vchirawongkwin, C. Kritayakornupong and B. M. Rode, *J. Phys. Chem. B*, 2010, **114**, 11561–11569.

32 V. Vchirawongkwin, C. Kritayakornupong, A. Tongraar and B. M. Rode, *J. Phys. Chem. B*, 2011, **115**, 12527–12536.

33 V. Vchirawongkwin, C. Pornpiganon, C. Kritayakornupong, A. Tongraar and B. M. Rode, *J. Phys. Chem. B*, 2012, **116**, 11498–11507.

34 J. M. Howell, A. M. Sapse, E. Singman and G. Snyder, *J. Phys. Chem.*, 1982, **86**, 2345–2349.

35 A. Banerjee, R. Shepard and J. Simons, *J. Chem. Phys.*, 1980, **73**, 1814–1826.

36 M. J. Frisch, G. W. Trucks, H. B. Schlegel, G. E. Scuseria, M. A. Robb, J. R. Cheeseman, J. A. Montgomery, T. Vreven, K. N. Kudin, J. C. Burant, J. M. Millam, S. S. Iyengar, J. Tomasi, V. Barone, B. Mennucci, M. Cossi, G. Scalmani, N. Rega, G. A. Petersson, H. Nakatsuji, M. Hada, M. Ehara, K. Toyota, R. Fukuda, J. Hasegawa, M. Ishida, T. Nakajima, Y. Honda, O. Kitao, H. Nakai, M. Klene, X. Li, J. E. Knox, H. P. Hratchian, J. B. Cross, V. Bakken, C. Adamo, J. Jaramillo, R. Gomperts, R. E. Stratmann, O. Yazyev, A. J. Austin, R. Cammi, C. Pomelli, J. W. Ochterski, P. Y. Ayala, K. Morokuma, G. A. Voth, P. Salvador, J. J. Dannenberg, V. G. Zakrzewski, S. Dapprich, A. D. Daniels, M. C. Strain, O. Farkas, D. K. Malick, A. D. Rabuck, K. Raghavachari, J. B. Foresman, J. V. Ortiz, Q. Cui, A. G. Baboul, S. Clifford, J. Cioslowski, B. B. Stefanov, G. Liu, A. Liashenko, P. Piskorz, I. Komaromi, R. L. Martin, D. J. Fox, T. Keith, A. M. A. Laham, C. Y. Peng, A. Nanayakkara, M. Challacombe, P. M. W. Gill, B. Johnson, W. Chen, M. W. Wong, C. Gonzalez and J. A. Pople, *Gaussian 03, Revision E.01*, Gaussian, Inc., Wallingford, CT, 2004.

37 N. Lee, R. G. Keesee and J. A. W. Castleman, *J. Chem. Phys.*, 1980, **72**, 1089–1094.

38 T. H. Dunning, Jr. and P. J. Hay, in *Gaussian Basis Sets for Molecular Calculations*, ed. H. F. Schaefer III, Plenum Press, New York, 1977, vol. 3, ch. 1, pp. 1–27.

39 T. H. Dunning, Jr., *J. Chem. Phys.*, 1970, **53**, 2823–2833.

40 H. J. C. Berendsen, J. P. M. Postma, W. F. van Gunsteren, A. DiNola and J. R. Haak, *J. Chem. Phys.*, 1984, **81**, 3684–3690.

41 F. H. Stillinger and A. Rahman, *J. Chem. Phys.*, 1978, **68**, 666–670.

42 P. Bopp, G. Janscó and K. Heinzinger, *Chem. Phys. Lett.*, 1983, **98**, 129–133.

43 S. Vchirawongkwin and V. Vchirawongkwin, *Comput. Theor. Chem.*, 2011, **974**, 26–30.

44 T. S. Hofer, H. T. Tran, C. F. Schwenk and B. M. Rode, *J. Comput. Chem.*, 2004, **25**, 211–217.

45 D. Xenides, B. R. Randolf and B. M. Rode, *J. Chem. Phys.*, 2005, **122**, 174506.

46 A. J. Lock, S. Woutersen and H. J. Bakker, *J. Phys. Chem. A*, 2001, **105**, 1238–1243.

47 P. Bopp, *Chem. Phys.*, 1986, **106**, 205–212.

48 D. E. Irish and R. V. Thorpe, *Can. J. Chem.*, 1975, **53**, 1414–1423.

49 M. H. Brooker and D. E. Irish, *Can. J. Chem.*, 1971, **49**, 1289–1295.

50 O. Lamba and H. Bist, *J. Phys. Chem. Solids*, 1983, **44**, 445–452.

51 L. A. Curtiss, K. Raghavachari, P. C. Redfern, V. Rassolov and J. A. Pople, *J. Chem. Phys.*, 1998, **109**, 7764–7776.

52 Y. Marcus, *J. Chem. Soc. Faraday T.*, 1991, **87**, 2995–2999.

53 A. Luzar and D. Chandler, *J. Chem. Phys.*, 1993, **98**, 8160–8173.
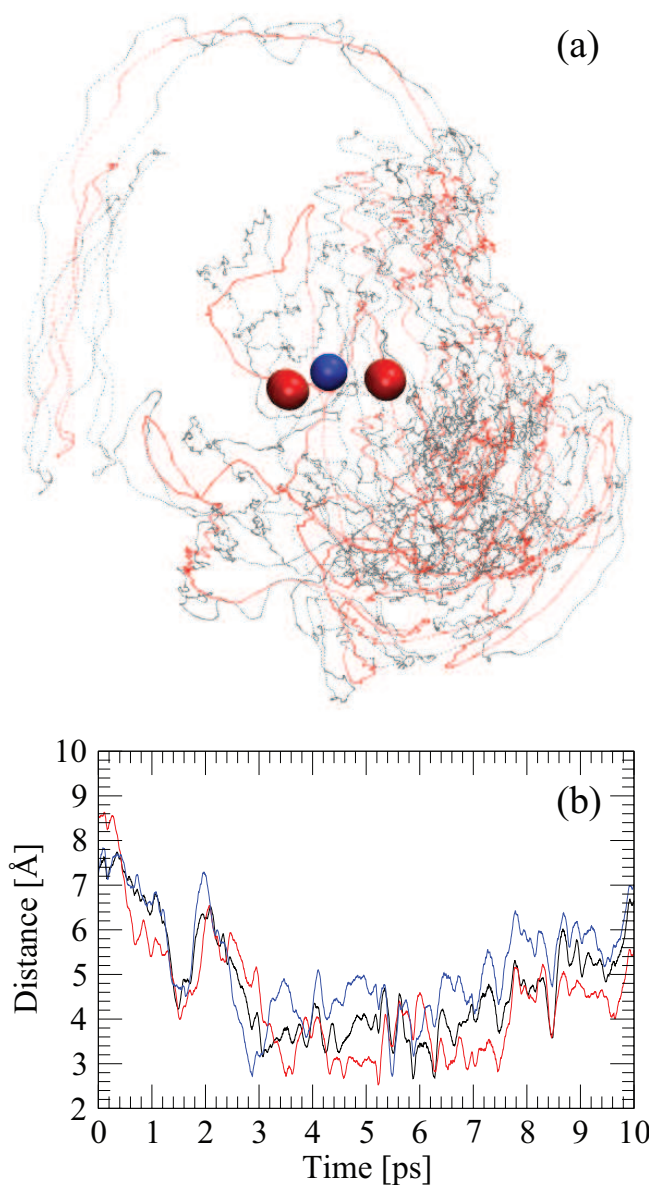
Fig. 8 (a) All superimposed trajectories for the coordination of the selected water with 3D alignment. The blue and red spheres are nitrogen and oxygens of NO_2^-, respectively, red and gray dots are the oxygen and hydrogens of the water. (b) Distances plot of the corresponded water molecule evaluated from N (black solid line), O(1) (red solid line) and O(2) (blue solid line) sites as a function of time during the QMCF MD simulation period.
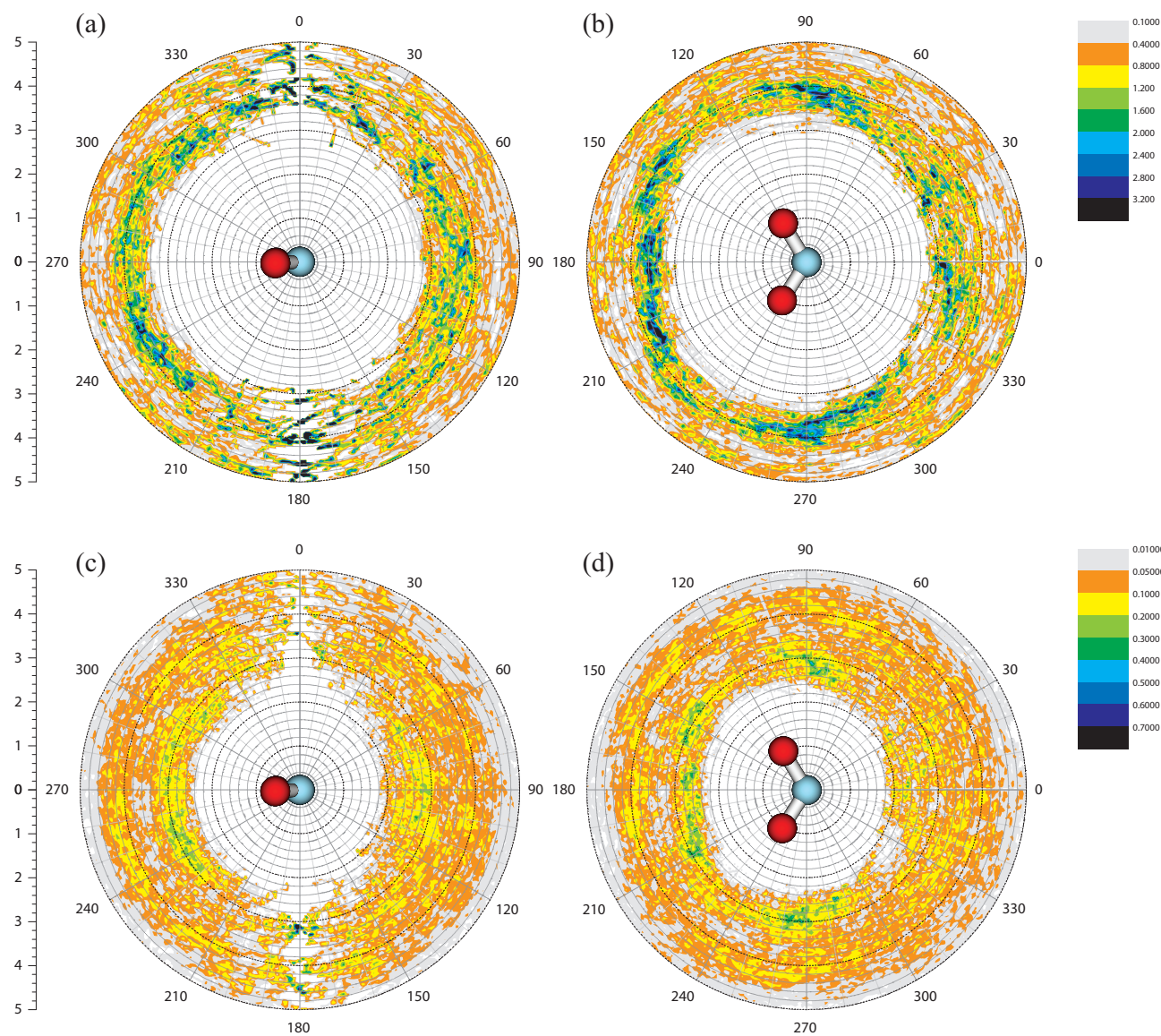
Fig. 6 Density maps of water molecules within 5 Å of hydration sphere projected onto (a) the (r,θ) and (b) the (r,ϕ) plane for the O atom, and (c) the (r,θ) and (d) the (r,ϕ) plane for H atom. The color bars present values of density in the unit of $g \cdot cm^{-3}$.
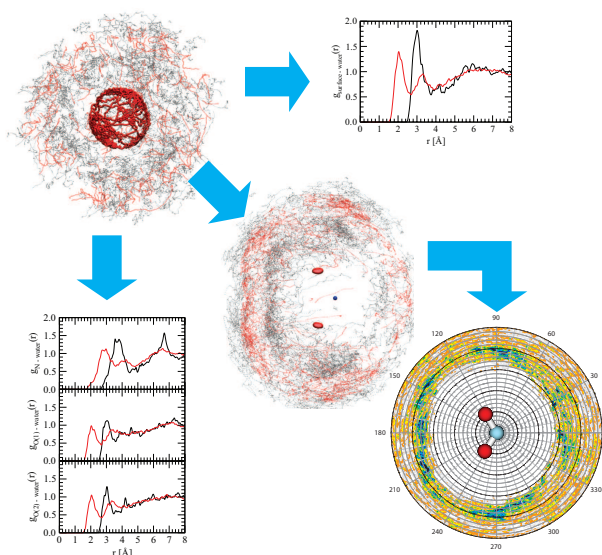
The quantum mechanical charge field molecular dynamics simulation (QMCF MD) unleashed the role of hydration shell to determine the reactivity of nitrite ion in an aqueous solution. However, the quantitative analysis of trajectories needs a rigorous method to organize the chaotic data into the informative data, clarifying an anisotropy of hydration structure. The results in this study suggested the steric effects of water in the bond direction.

1